

Introduction

Lithography Roadmap

Year	2001	02	03	04	05	06	07	08	09	10	11	12	13
Technology Node	130	90	65	45	32								
LWR (nm)			3.4	2.4	1.7								
Lithography Solution	KrF (248 nm)	ArF excimer (193nm)	ArF excimer (193nm)	ArF excimer (193nm)	EUV (13.5nm)								
					Electron beam for mask production								

Figure 1 International Roadmap for Semiconductor (ITRS) 2005, lithography.

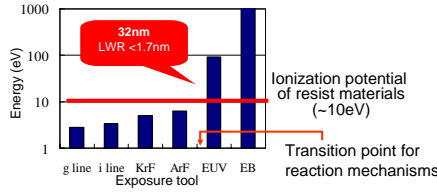


Figure 2 Photon energies of the exposure tools.

Toward 32 nm technology node, the development of next generation lithography such as electron beam (EB) and extreme ultraviolet (EUV) lithographies has been pursued; however, the feature sizes and accuracy become close to the performance limit of resist materials. The development of chemically amplified (CA) resists applicable to mass production lines of 32 nm technology node has emerged as the most critical issue. Fundamental understanding of the pattern formation mechanism is strongly required to meet all the criteria such as sensitivity, resolution, and etching resistivity. Among the requirements, the reduction of line edge roughness (LER) or line width roughness (LWR) appears to be the most challenging issue. The mechanisms of LER formation have been subjected to intensive investigations in the lithography community. Numerous factors related to aerial image quality, resist process and materials have been reported. It has been widely accepted that the process and material factors become critical when the image quality is degraded. Since the image quality produced by EB and EUV is potentially higher than that produced by deep UV, the LERs in EB and EUV lithographies are expected to become small. Nevertheless, significant LER has still been observed and remains the most serious problem in EB and EUV resists.

It has been elucidated by our group that the use of ionizing radiation such as EB and EUV changes the change of acid formation mechanism in CA resists, which gives rise to an additional factor to cause resolution blur. When an ionizing radiation passes the resist materials, it randomly deposits the energy to resist materials via ionization and excitation of resist components. Among these energy deposition processes, the ionization of polymer plays the most important role in acid generation. The electrons generated by ionization events lose their kinetic energy through the interaction with surrounding molecules to thermal energy level (thermalization) and gives a narrow distribution around their parent radical cations. Many kinds of photo acid generators (PAGs) can react with the low energy electrons and produce counter anions of acids, which leads to the spatial discrepancy between ionization point (proton-generated point) and counter anion-generated point. The reaction history intrinsic to these reaction mechanisms has also significant impact on the LER formation. The initial proton and counter anion distribution were calculated on the basis of the formulation of acid generation through polymer ionization. Although the protons are generated at ionization point, the counter anion distribution is significantly wider than proton distribution. The counter anions are inhomogeneously distributed outside a relatively smooth edge of proton distribution.

We previously reported the effects of the initial acid distribution and subsequent acid diffusion on the LER formation of latent images with the exposure range from 1 to 5 $\mu\text{C}/\text{cm}^2$. It was elucidated that the proton distribution boundary was deformed by the inhomogeneous anion distribution. The subsequent acid diffusion smoothed out the initial roughness of acid distribution by about 25%. In this study, the previous work is extended to the exposure dose of 50 $\mu\text{C}/\text{cm}^2$. With the increase of exposure dose, the statistical effect, i.e. shot noise is expected to decrease, although the effect of image contrast slope still remains. The dependences of LER and image contrast slope on the high exposure dose are examined, demonstrating the correlation between LER and the fluctuation in the initial number of acid molecules generated in resists.

What happen in the nanoscale patterning ?

What is the mechanism of LER formation in CA resists of EUV and EB lithographies?

Radiation chemical reaction in resist

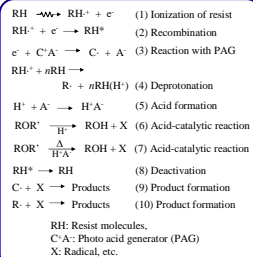


Figure 3 Line and space pattern of chemically amplified resist fabricated by electron beam lithography. Roughness of the line edges can be seen.

Brief explanation of the reactions

Reaction (1) is very fast on the femtosecond time scale or faster than that. Photochemical reaction, e.g. (CA⁺)⁺ is minor path in ionizing radiation. Reaction (2) and (3) is why- and how- and protonic time scale. These reactions can be directly observed by subpicosecond pulse radiolysis. By analyzing the kinetic traces of RH⁺ or e⁻ using Smolochowski equation, we can experimentally obtain evolution of their spatial distributions. Reaction (4) is much faster than reaction of proton and counter anion during reaction (5) can be simulated using initial spatial distributions of proton and counter anion. Initial concentration of proton was experimentally measured.

Results and Discussions

The initial spatial distributions of protons (green) and counter anions (red) produced upon 10, 20, and 50 $\mu\text{C}/\text{cm}^2$ exposure to EB are depicted in Fig. 1. The roughness of proton distribution is moderated with the increase of exposure dose, while the number of counter anion existing in outer area seems increased. This is simply due to the statistical phenomenon. The following two paragraphs discuss the detail of the meaning of "statistical".

The initial fluctuation between protons and counter anions in the same area was obtained by solving Smolochowski equation (diffusion under Coulomb potential) in the presence of electron scavenger (PAG). We found that the calculated initial distribution function $f(r)$ can be empirically fitted by

$$f(r) = A \left[1 - e^{-r/R_{eff}} \right] e^{-r/R_p} \quad (1)$$

where r and R_{eff} are the distance between proton and anion in spherical coordinate and the effective reaction radius between proton and anion, respectively. Note that $f(r)$ is zero if r is less than R_p . A , R_p , and R_{eff} are the fitting parameters. In the case of resist system adopted in this paper, the least-square fitting resulted in $A = 0.272$ (no unit, scaling factor), $R_p = 1.70$ nm, and $R_{eff} = 3.91$ nm. The average distance $\langle r \rangle$ was calculated by

$$\langle r \rangle = \frac{\int_0^\infty r f(r) dr}{\int_0^\infty f(r) dr} = R_p + r_1 + \frac{r_2}{r_1 + r_2} \quad (2)$$

giving $\langle r \rangle = 5.6$ nm. The r_2 is close to the average distance of thermalized electrons in which a single exponential function with average distance (4 nm) was assumed. The expansion of average distance of anion by 1.6 nm from 4 nm is ascribed to the simulated charge recombination between radical cations of resist polymer and thermalized electrons in short-distance area. This recombination is much faster than both proton-anion encounter and electron-PAG reaction, because the diffusion coefficient of the thermalized electrons is a few to several orders of magnitude larger than that of proton and attractive force between radical cations and electrons is considerably strong. Therefore, the proton-anion distribution expressed by Eq. (2) can be treated as already formed before the acid formation process proceeds.

It is manifest that the tail of initial distribution $f(r)$ is nearly identical to an exponential, and thus, the probability of counter anion production is significantly reduced with the increase in the distance r . Therefore at the low exposure dose, it is a rare case that counter anions exist in such the small probability region (tail) of the distribution, at the high exposure dose, the number of counter anions statistically increases, forming a more scattered feature of the distribution. Since the counter anions pull out protons and deform the boundary of latent image, a larger exposure dose might degrade the LER of latent image. On the other hand the increase of exposure dose has opposite effect, i.e. an improvement of LER, because of the sharpening of the edge contrast. The total effect of exposure dose on the latent image is discussed later in this paper.

Figure 2 shows a correlation between line width (LW) and LER (3 σ) of latent images during PEB. In most of the curves, the LER decreases with an increase of line width, reaching minimum point of LER, and then increases. This down-and-up phenomenon is understood as a smoothing effect by acid diffusion as is also observed at lower exposure doses. The smoothing effect is caused if there is an edge roughness of latent image before PEB. The roughness is formed during the acid formation process in which protons migrate with catalyzing deprotection reactions and stabilized by immobile counter anions.

The amine concentration was set to 0.4 or 1.0 relative to the initial concentration of proton-counter anion pairs. In the adopted resist system, the relative concentration of amine celer is approximately given by

$$c_{rel} = \frac{4100 \lambda^2}{M} \quad (3)$$

where M , λ , and D are the density of the resist polymer, the molecular weight of amine, concentration of amine in wt%, and exposure dose in $\mu\text{C}/\text{cm}^2$ unit, respectively. Note that this approximation is not valid if one of the parameters such as the PAG concentration, the initial concentration of proton-counter anion pairs, and the initial average distance between thermalized electron and radical cation is changed. If the dependence of LW-LER curves on exposure dose is compared at the same relative amine concentration, one can find that the curve shifts towards shorter line width and smaller LER. This LER improvement is caused by combination of edge contrast enhancements by increase of amine and decrease of edge fluctuation by increase of dose.

The LW-LER curve is shortened by increasing the relative amine concentration from 0.4 to 1.0 for all exposure doses, and the degree of the shortening seems larger for higher exposure dose. The length of the curve reflect a margin of acid diffusion, that is, a longer curve means the number of surviving acids is large enough to promote more catalytic reactions during PEB. Although the concentration of amine was increased by raising exposure dose, we also increased the amine concentration according to Eq. (4) to retain the relative concentration constant. This protocol results in the increase of probability that acids encounter a large number of amine when the acids migrate outward. If whether the concentration of acids or amines is much smaller than the other, and thus, the latter can be regarded as constant, the change in the length of LW-LER curve would be observed. The concentrations are also understood as the result of shot noise reduction. Therefore, quenching rate of acids is accelerated due to a second-order effect by the increase in exposure dose.

Examples of 3D latent images at the minimum LER points are drawn in Figs. 2b, c, and d. The relative amine concentration is 1.0. One can see smaller number of fitting parameters. The blue- and green-colored meshes represent catalyzed area by protons and acids, respectively. In this paper we assumed that the activation energy of deprotection reaction is zero, which implies that at least single hit by proton or acid yields polarity change of the polymer substituent. This treatment is not realistic. Besides, the dissolution rate during development process depends on the deprotection rate in one polymer molecule. The correlation between line width and LER is reproduced from a feature projected on the plane perpendicular to EB irradiation, i.e. on the xy plane (see Fig. 1a). Thereby a long protracted trajectory is influential in the simulation results. Therefore the LERs found here would be much larger than those of positive-tone CA resist obtained by taking into account the activation energy and development process. These effects will be reported elsewhere. Although the LER after development would be reduced by such factors, the LERs of latent images affect the final feature topology and it is essential to reduce them for the achievement of advanced nanolithography in the forthcoming future.

Figure 3 shows the minimum LER dependence on exposure dose and amine concentration. The value in the bracket in Fig. 3a represents the relative concentration of amines to the initial concentration of proton-counter anion pairs. The solid lines are empirical fitting curves expressed by

$$\text{LER} = \alpha \left(\frac{4100 \lambda^2}{M} \right)^{\beta} \cdot D^{\gamma} \quad (4)$$

where α , β , and γ are the fitting parameters. Although other types of functions are, in actual, applicable, we used here the simplest function which has the smallest number of fitting parameters. In fact, the best fit was obtained using $\alpha = 16 \pm 1.4$, $\beta = -0.22 \pm 0.04$, and $\gamma = -0.26 \pm 0.04$. Equation (5) is rewritten as follows.

$$\text{LER} = \alpha' \left(\frac{4100 \lambda^2}{M} \right)^{\beta} \cdot c_{rel}^{\beta} \cdot D^{\beta-\gamma} \quad (5)$$

If the c_{rel} absolute concentration of amine (not relative concentration c_{rel}), is fixed, the LER obey $D^{-\beta}$, where the β was -0.04 ± 0.06 . Although the dependence of exposure dose indicated inverse proportionality, we can not readily conclude that increase of exposure dose at fixed c_{rel} enhance the LER of latent image, because the calculation error was large enough to be significant. Despite the β - γ fluctuated within the calculation error, the absolute value of $|\beta - \gamma|$ is still small, predicting that the dependence of the LER of a latent image on only exposure dose is not significant under the assumed conditions. The LER reduction is also understood as the result of shot noise reduction. On the contrary, according to Eq. (6) and the obtained value for β , amine concentration has distinguishable improvement of LER. It should be, however, noted that oversupply of amine yields a vermiculate latent image, leading to a failure of development. This is suggestive of adequate amine concentration to form normal line features. On the other hand, the increase of exposure dose enlarges the margin of involved amine concentration.

Figure 4 represents the image contrast for various exposure doses after a certain PEB time. The relative amine concentration is fixed at 0.4 for amine concentration. As can be expected from Eq. (5), the image contrast is improved with the exposure dose. While the catalyzed percentage at the curve edge of around 25 nm is constant, that at the center part (0 to 15 nm) increases with the exposure dose, resulting in the steeper slope of the edge contrast. Therefore, the improvement of LER by the increase of exposure dose at constant relative amine concentration is understood as the result of sharpening of the image contrast. In contrast to Fig. 4b, Figs. 4b in which absolute amine concentration is fixed at 0.5 wt% shows a different dependence on exposure dose. While the catalyzed percentage at the center increases with the exposure dose, the contrast curves spread outward. Normalized contrast curves were compared, showing almost identical feature. Consequently, the LER of latent image is not improved so much by increase of dose at fixed absolute amine concentration. It is, however, emphasized that reduction of LER at high exposure dose would appear if an activation energy of deprotection reaction and development process are incorporated into the simulation, because these are sensitive to both the top value and slope at the edge of the contrast curve.

The correlation between LER and shot noise is presented in Fig. 5. The shot noise is expressed here by the square root of N of Over N , where the N is the initial number of acid molecules generated in the LER width \times LER length \times 100 nm height. The correlation was obtained using this definition and Eq. (6) including the used fitting parameters α , β , and γ . The result clearly demonstrates the nearly linear correlation between the LER and shot noise. Note that we did not incorporate the fluctuation of the number of acid molecules, i.e. shot noise effect, in this simulation, although the blur of beam shape was taken into account. Thereby, the percentage shown in Fig. 5 represents the increase of LER at a certain LER. For instance, 15 nm LER would be degraded to ~ 16.5 nm ($\sim 10\%$ increase) due to the shot noise effect. This is suggestive of a small effect of the shot noise on the LER at high exposure dose.

Therefore we conclude that the enhancement of the image contrast rather than the reduction of shot noise predominantly account for the improvement of LER of latent image at high exposure dose. In addition, the increase of exposure dose raise the upper limit of applicable amine concentration which has significant effect on the enhancement of image contrast, and thereby reduction of LER of latent image.

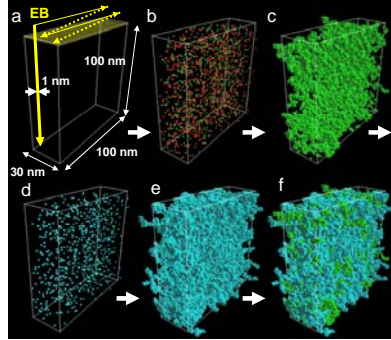


Figure 4 Scheme of Monte Carlo simulation in the case of 2 $\mu\text{C}/\text{cm}^2$ exposure with 0.2 wt% amine. (a) Exposure of 75-keV electron beam (EB) in a 30 \times 100 \times 100 nm area. The trajectories of EB were calculated by SELD (see Methods). (b) Initial distribution of protons (green) and counter anions (red). (c) Latent image formed by proton migration during acid formation process. The mesh was a 1-nm cube. (d) Initial distribution of acids before post-exposure bake (PEB). (e) Latent image formed by acid diffusion after PEB. (f) Final latent image formed by proton migration (green) and acid diffusion after PEB (blue).

Simulation scheme of reaction (5)-(7): acid formation and acid diffusion

The Monte Carlo simulations were executed by an in-house software reported previously. A brief description of the simulation is as follows. A 75 keV electron beam of which shape was assumed Gaussian with 1 nm was deposited to a resist film Poly(4-hydroxyethylene) (PHE), density = 1.2 g/cm³, dielectric constant = 4) was chosen as a typical CA resist. The film thickness and exposed area were 100 nm and 30 nm wide \times 100 nm long, respectively. The exposure doses were varied by changing the scan speed of the beam, giving 1, 2, 5, 10, 20, and 50 $\mu\text{C}/\text{cm}^2$. The initial concentrations of protons and electrons were based on experiments, in which they were estimated by dependence of photo-absorbance of proton-adducts on the dye concentration. After protons originating from radical cation of resists were distributed randomly along the primary and secondary electron beams, counter anions generated via electron capture by photo acid generator (PAG, 10 wt%) were distributed around the protons. The initial distribution of distances between the ionization point and counter anion was estimated from analysis of kinetic traces measured by pulse radiolysis. The average distance between the proton and thermalized electron was 4 nm and the counter anions were distributed isotropic to the proton position.

To trace the dynamics of hundreds of proton and counter anion produced by EB/EUV, we adopted a Monte Carlo technique. The motion of charged particles for each time step Δt is given by

$$\Delta \mathbf{r}_i = \sqrt{D_i \Delta t} \mathbf{u}_i + \mu_i \sum_j \mathbf{E}_j \Delta t \quad (1)$$

where D_i , μ_i , and \mathbf{E}_j represent the diffusion coefficient of the i -th charged particle, the uniform random variable from -1 to 1, the mobility of the i -th charged particle, and the electric field produced between the i -th charged particle and the j -th charged particles, respectively. Once the distance between proton and counter anion becomes less than the reaction radius r_c , proton and counter anion recombine to generate an acid. In the simulations, the unit of time is, actually, converted to a non-dimensional variable.

The spherical amine molecules were distributed randomly in the resist, changing the number of molecules according to the amine concentration. During proton migration, if the distance between proton and amine molecule became less than 0.5 nm, the protons were scavenged, fixing the positions of the positive charges throughout the calculation. The diffusion coefficient of the bulky counter anion was zero during proton migration, because it is negligibly small compared to that of protons at room temperature. Calculations were stopped after all protons disappeared after amine scavenging reactions. The trajectories of protons were recorded and used to produce a latent image. The mesh size used for the reproduction of latent images was a 1-nm cube. After the calculations for acid formation, acid diffusion during PEB was calculated. The motion of the acid is reproduced by Eq. (1), with the second term of the right side of the equation being zero.

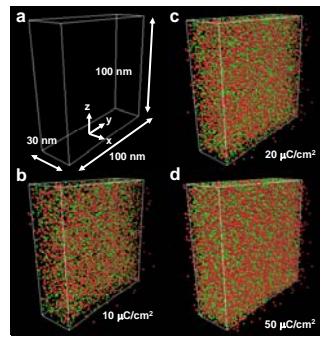


Figure 1 Initial distribution of protons (green) and counter anions (red) produced upon 10, 20, and 50 $\mu\text{C}/\text{cm}^2$ exposure to EB. (a) Dimension of the irradiated area by EB. The exposure doses are (b) 10 $\mu\text{C}/\text{cm}^2$, (c) 20 $\mu\text{C}/\text{cm}^2$, and (d) 50 $\mu\text{C}/\text{cm}^2$.

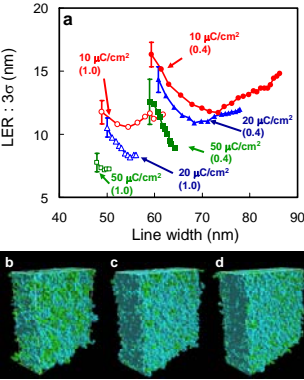


Figure 2 (a) Correlation between the line width and LER (3 σ) after PEB process for 10, 20, and 50 $\mu\text{C}/\text{cm}^2$ exposure doses. The values in the brackets represent ratio of amine (quencher) concentration to the initial concentration of proton-counter anion pairs. The 3D images are latent images of deprotected area catalyzed by protons and acids at the minimum LER points for (b) 10 $\mu\text{C}/\text{cm}^2$, (c) 20 $\mu\text{C}/\text{cm}^2$, and (d) 50 $\mu\text{C}/\text{cm}^2$. The amine ratio is 1 relative to initial proton-counter anion pairs.

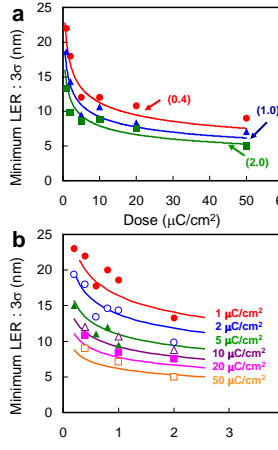


Figure 3 (a) LER dependence on exposure dose. The values indicated with arrows represent the ratio of the concentration of initial proton-counter anion pairs to that of amine (quencher). (b) LER dependence on the relative concentration of amine to the concentration of initial proton-counter anion pairs. The closed circles, open circles, closed triangles, open circles, closed squares, and open squares represent exposure doses of 1, 2, 5, 10, 20, and 50 $\mu\text{C}/\text{cm}^2$, respectively.

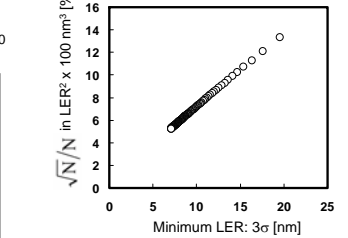


Figure 5 Correlation between the minimum LER and shot noise.

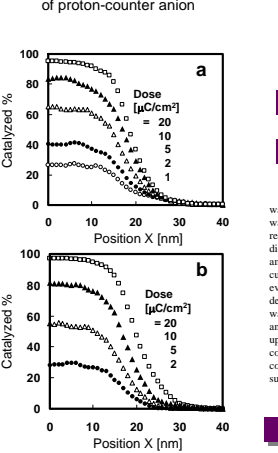


Figure 4 Image contrast curves by changing exposure dose after PEB. (a) The relative amine concentration to the initial proton-counter anion pairs was fixed as 0.4 for each exposure dose. (b) The absolute amine concentration was fixed as 0.5 wt%.

Summary

The exposure dose dependence on the LER of latent images in an EB-CA resist was investigated by a Monte Carlo simulation. The effect of amine on the LER was analyzed by the empirical equation, and image contrasts were calculated. The results demonstrated that increase in exposure dose at a fixed amine concentration did not exhibit significant reduction of the LER, while that at a fixed relative amine concentration to the initial proton-counter anion sharpened the contrast curve, and thus, decreased the LER. The image contrast is expected to be enhanced even at a fixed amine concentration by incorporating activation energy and development process into the simulation. The contribution of shot noise to LER was found small, compared to the blur caused by the initial separation of protons and counter anions. One of the advantages of high exposure dose is the raise of upper limit of applicable amine concentration. High amine concentration can considerably improve the LER of latent image, while excessive amine concentration disables the development of feature topology due to the lack in sufficient polarity change of resist polymer.

Publications

- "Line-edge roughness of a latent image in post-optical lithography" Δ Saeki, T., Kozawa, S., Tagawa, and H. B. Cao, *Nanotechnology*, **17**, 1543 (2006).
- "Correlation between proton dynamics and line edge roughness in chemically amplified resist for post-optical lithography" Δ Saeki, T., Kozawa, S., Tagawa, and H. B. Cao, *J. Vac. Sci. Technol. B*, submitted.
- "Multi-sputter effect on decay kinetics of geminate ion recombination using Monte Carlo technique" Δ Saeki, T., Kozawa, Y., Yoshida, and S. Tagawa, *Appl. Instrum.*, **6**, 660, B34, 283 (2005).
- "Proton and anion distribution and line edge roughness of chemically amplified electron beam resist" T. Kozawa, H. Yamamoto, Δ Saeki, and S. Tagawa, *J. Vac. Sci. Technol.*, **B23**, 2716 (2005).
- "Modeling and simulation of chemically amplified electron beam, x-ray and EUV resist processes" T. Kozawa, Δ Saeki, and S. Tagawa, *J. Vac. Sci. Technol.*, **B22**, 3489 (2004).
- "Relation between spatial resolution and reaction mechanism of chemically amplified resists for electron beam lithography" T. Kozawa, Δ Saeki, A. Nakano, and S. Tagawa, *J. Vac. Sci. Technol.*, **B21**, 3149 (2003).
- "Study on Radiation-Induced Reaction in Microscopic Region for Basic Understanding of Electron Beam Patterning in Lithographic Process (II) - Relation between Resist Space Resolution and Space Distribution of Ionic Species -" Δ Saeki, T., Kozawa, Y., Yoshida, and S. Tagawa, *Jpn. J. Appl. Phys.*, **41**, 4213 (2002).